Available online at www.sciencedirect.com
ScienceDirect
Journal of Power Sources 165 (2007) 34–40
JOURNAL OF POWER SOURCES
www.elsevier.com/locate/jpowsour

High-performance (La,Sr)(Cr,Mn)O_3/(Gd,Ce)$O_{2-\delta}$ composite anode for direct oxidation of methane

X.J. Chen *, Q.L. Liu, K.A. Khor, S.H. Chan

Fuel Cell Strategic Research Programme, School of Mechanical and Aerospace Engineering, 50, Nanyang Avenue, Nanyang Technological University, Singapore 639798, Singapore

Received 22 August 2006; accepted 16 November 2006
Available online 12 January 2007

Abstract

A novel (La,Sr)(Cr,Mn)O_3/(Gd,Ce)$O_{2-\delta}$ (LSCM/GDC) composite electrode is developed and applied as solid oxide fuel cell (SOFC) anode for direct oxidation of methane. The optimum composition of the composite anode is 33 wt.% LSCM and 67 wt.% GDC. At an output current density of 0.5 A cm^{-2}, the overpotential of the anode in wet H_2 and CH_4 at 850 °C is 0.073 and 0.248 V (i.e., an anodic resistance of 0.146 and 0.496 Ω cm^2), respectively. The oxidation of CH_4 on the composite anode is primarily studied by means of electrochemical impedance spectroscopy under different temperatures and a dc bias. The stability of the LSCM/GDC composite anode is evaluated under different current loadings in wet CH_4 at 850 °C for 50 h. The results show that the developed LSCM/GDC composite anode has high stability in CH_4 fuel and possesses good electrochemical performance that is comparable with a Ni cermet anode.

Keywords: Solid oxide fuel cell; Perovskite; Methane oxidation; Anode; Stability; Electrochemical performance

1. Introduction

Advances in electro-ceramics, such as ionic conductors and electronic/ionic mixed conductors, are critical to the development of solid oxide fuel cell (SOFC) technology. The advantages of SOFCs over other types of fuel cell reside in the following: (i) flexible selection of fuels, i.e., hydrogen, natural gas, bio-gas and liquid hydrocarbons; (ii) diminished electrolyte-management problems because of the use of ceramic components; (iii) tolerance to poisonous gases, i.e., CO and H_2S. Although hydrogen is the most appropriate fuel for SOFC to achieve high performance, it can only be obtained through reforming of hydrocarbons, electrolysis or photo-electrolysis [1–3]. Economically, it is ideal to use any hydrocarbons directly instead of being converted to hydrogen as the fuel for SOFCs. Methane, as the simplest compound among the hydrocarbons, is one of the most preferred hydrocarbons and is abundant in the form of natural gas.

Nickel is a good anode material for SOFCs, but the formation of coke during direct reforming makes it unattractive. A high molar steam-to-methane ratio has to be used to prevent possible coke formation at the Ni/YSZ anode and this causes dilution of reformed hydrogen. Many researchers have focused their studies on the internal reforming and the stability of the SOFC anode in methane fuel [4–10]. A major challenge for the direct use of methane is to suppress carbon deposition at the anode. Currently, two alternative anodes, i.e., Cu-based cermet and perovskite materials, have been developed as Ni-free SOFC anodes that can directly operate in hydrocarbon fuels with performances comparable with that of nickel cermet. Gorte and co-workers [11–13] has published a series of papers on the use of Cu–ceria cermet to avoid carbon deposition in the hydrocarbon fuels at operating temperatures in the range of 500–700 °C. Lanthanum chromites ($LaCrO_3$) have been intensively investigated as interconnects for SOFCs due to their stability in both an oxidizing and a reducing environment at high operating temperatures. Substitution of alkaline earth ions (Mg, Ca, Sr) into the A-site of $LaCrO_3$ can enhance the electrical conductivity by two orders of magnitude [13]. Introducing transition elements (Cu, Mn, Fe, Ti, Ni, V) into the B-site of the $LaCrO_3$ can improve the catalytic activity and ionic conductivity [14–17], parameters that are crucial for the perovskite anode to oxidize hydrocarbons, electrochemically.

* Corresponding author. Tel.: +65 67904192; fax: +65 67905591.
E-mail address: chenxj@pmail.ntu.edu.sg (X.J. Chen).

0378-7753/$ – see front matter © 2006 Elsevier B.V. All rights reserved.
doi:10.1016/j.jpowsour.2006.11.075

A series of Sr-doped lanthanum chromites with introduction of transition elements at the B-sites has been investigated as SOFC anodes. The $La_{0.7}Sr_{0.3}Cr_{0.8}Ti_{0.2}O_3$ [18] and $La_{0.8}Sr_{0.2}Cr_{0.97}V_{0.03}O_{3\pm\delta}$ [19] have been studied and found to have anode polarization resistances around 40 and 2.1 $\Omega\,cm^2$ in wet H_2 at 850 °C, respectively. The anode polarization resistance of another perovskite, $La_{0.75}Sr_{0.25}Cr_{0.5}Fe_{0.5}O_3$ (LSCrF), has been reported to be 1.15 $\Omega\,cm^2$ in wet H_2 at 850 °C [17]. The observed performance of the above materials is not comparable with that of the state-of-the-art Ni cermet. Recently, Tao and Irvine [20] investigated a (La,Sr)(Cr,Mn)O_3 (LSCM) anode, which is chemically stable in a natural gas or methane environment and has comparable performance with nickel/YSZ. The polarization of the $La_{0.75}Sr_{0.25}Cr_{0.5}Mn_{0.5}O_3$/YSZ composite anode was reported to be 0.26 and 0.87 $\Omega\,cm^2$ in wet H_2 and CH_4 with a graded anode at 900 °C, respectively. Liu et al. [21] have developed a $Ce_{0.9}Gd_{0.1}O_{1.95}$ electrolyte-supported single cell using LSCM–GDC–Ni as the anode [21]. A maximum power density of 0.16 and 0.12 W cm^{-2} was achieved at 750 °C in H_2 and C_3H_8 fuels, respectively. The best electrochemical performance shown by the perovskite with Mn substitution at the B-site may be attributed to the ability of Mn to accept lower coordination numbers in perovskite and to the p-type conduction of Mn, that results in mixed electronic/ionic conduction.

The Sr-doped lanthanum chromites are quite stable in hydrogen and hydrocarbon fuels. Nevertheless, success in applying the perovskite materials as anodes in SOFCs depends on the level of performance that the perovskite anode can achieve. Besides the characterstic properties of the materials, e.g., catalytic activity, electrochemical activity, ionic and electronic conductivity, the microstructure of the anode also plays an important role in seeking an improvement in performance. The use of materials with fine particle size can dramatically increase the ionic-electronic-fuel three-phase-boundary and thus greatly enhance the efficiency of the anode. This study concerns the development of a high-performance GDC/LSCM composite anode for the direct oxidation of methane. The $La_{0.75}Sr_{0.25}Sr_{0.5}Cr_{0.5}O_3$ powder is synthesized through a combined citrate and EDTA complexing method and then applied to the composite anode.

2. Experimental

Discs of yttria-stabilized zirconia electrolyte (YSZ) were prepared by uniaxially compacting pressing of 8 mol% yttria-stabilized zirconia powder (Tosoh Corporation, Japan) at a pressure of 50 MPa and then sintering at 1550 °C for 2 h. The sintered YSZ electrolyte disc was 1 mm in thickness and 18 mm in diameter. The $La_{0.75}Sr_{0.25}Cr_{0.5}Mn_{0.5}O_3$ perovskite powder was synthesized through a combined citrate and EDTA complexing method, a flowchast of the procedure is given in Fig. 1. The chemicals, $Cr(NO_3)_3{\cdot}9H_2O$, $Sr(NO_3)_2$, $Mn(NO_3)_2{\cdot}4H_2O$, $La(NO_3)_3{\cdot}6H_2O$, EDTA, and citric acid, were all obtained from Sigma–Aldrich. Necessary amounts of $Cr(NO_3)_3{\cdot}9H_2O$, $Sr(NO_3)_2$, $Mn(NO_3)_2{\cdot}4H_2O$, $La(NO_3)_3{\cdot}6H_2O$ were dissolved in EDTA-$NH_3{\cdot}H_2O$ solution under heating and stirring. When all the nitrates had dissolved, an appropriate amount of citric acid was introduced at a molar ratio of EDTA acid:citric acid:total metal ions of 1:1.5:1. After condensation of the solution, a dark purple gel was formed. The gel was then heated at 130 °C for several hours to form a powder precursor, which was then calcined at 800 °C for 5 h to obtain the LSCM powder. X-ray diffraction (XRD) patterns of $La_{0.75}Sr_{0.25}Cr_{0.5}Mn_{0.5}O_3$ powders synthesized by a solid-state reaction and the sol–gel method, given in Fig. 2. The peaks for the powder synthesized by the sol–gel method are much wides than those for powder obtained by a solid-state reaction. This indicates that the former route produces a finer particle size. From the XRD results, it is confirmed that the synthesized powder has a perovskite structure with the phase composition being same as that obtained by Tao and Irvine [22]. For the solid-state reaction, a calcination temperature higher than 1100 °C is required for the formation

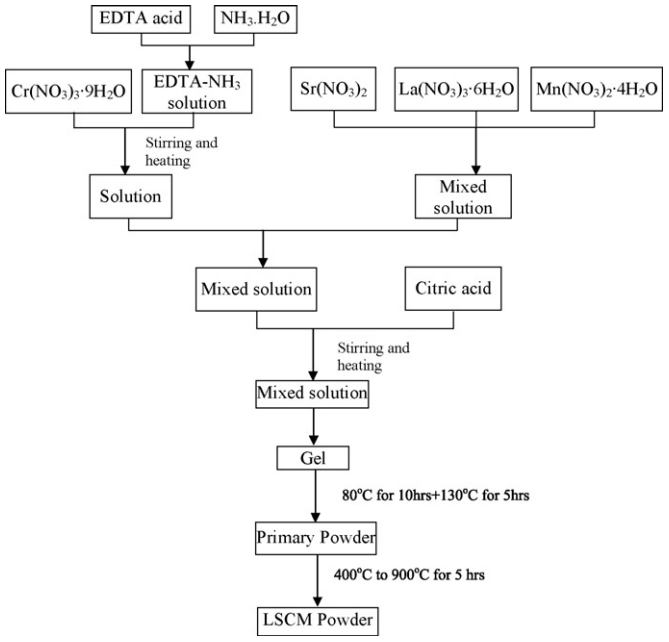

Fig. 1. Flowchart of LSCM powder synthesis.

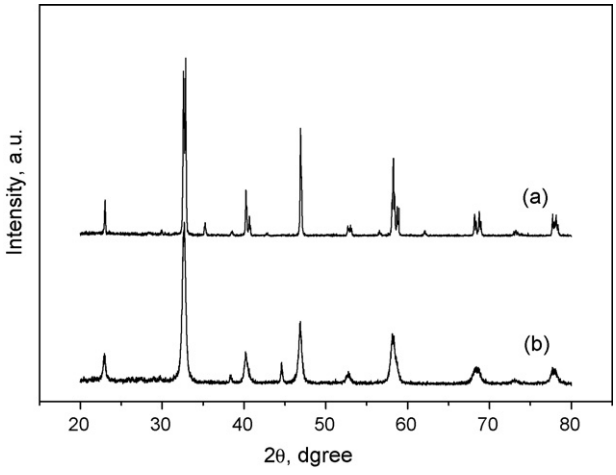

Fig. 2. XRD patterns of LSCM powder synthesized by (a) solid-state reaction (pre-sintered at 1300 °C for 10 h) and (b) sol–gel method (pre-sintered at 800 °C for 5 h).

of the perovskite phase [22]. In the present study, the perovskite phase is formed at a calcination temperature as low as 500 °C when using a gel precursor. This may be attributed to the formation of a homogenous multicomponent gel without any phase segregation during the processing. Thus, the fine grain size of the LSCM powder produced by the sol–gel method is expected because of the low calcination temperature.

The LSCM and GDC powders (from NexTech with an average particle size of 50 nm) were mixed intimately with polyethylene glycol 400 to form a slurry, which in turn was screen-printed onto the YSZ electrolyte surface and then sintered at 1000 °C for 2 h in air to produce the $(La,Sr)(Cr,Mn)O_3/(Gd,Ce)O_{2-\delta}$ composite anode. The thickness of the anode after sintering was around 50 μm and the surface area was 0.5 cm^2. Platinum paste was coated on the other side of the YSZ electrolyte to serve as the counter and reference electrodes, followed by sintering at 1000 °C for 1 h. During experiments, the counter and reference electrodes were exposed to air, while the anode was exposed to a wet methane (or wet hydrogen) atmosphere. The electrochemical measurements were performed on the composite anode in wet H_2 and CH_4 over a temperature range of 700–900 °C by means of impedance spectroscopy and current–voltage (*I–V*) polarization (Autolab, Netherlands). The applied frequency was 0.01–10^6 Hz with an ac amplitude of 10 mV. Scanning electron microscopy (SEM, JOEL 350, Japan) was employed to observe the microstructure of the LSCM–GDC composite anode.

3. Results and discussion

3.1. Performance of LSCM–GDC composite anode

The performance of a composite electrode is strongly related to parameters, such as particle size, pore size, porosity and the volume ratio of the ionic and electronic conductors. Simulation results for LSM/YSZ composite cathodes have shown [23] that there exists an optimum volume ratio of LSM and YSZ in the composite cathode for certain particle sizes of the two components. For experimental convenience, the weight ratio in this study was chosen to optimize the LSCM/GDC composite anode. Due to the pseudo-inductive behaviour at low frequency of the impedance in wet CH_4 at a temperature of 850 °C (see Fig. 5(b) later), the electrode resistance at 0.5 V was used as a reference parameter to optimize the composite anode. The electrode resistance can be obtained as:

$$R_p = \frac{OCV - 0.5}{I} - R_e,$$

where I is the current density of the anode at 0.5 V, and R_p and R_e are the electrode resistance and the electrolyte resistance, respectively. As shown in Fig. 3(a), for changes in the weight percentage of LSCM from 25 to 50 wt.%, the minimum electrode resistance is 0.87, 0.65 and 0.5 Ω cm^2 at 33 wt.% LSCM in wet CH_4 at 750, 800 and 850 °C, respectively. This is due to the optimized contribution of the electronic and ionic conduction and the active reaction sites on the anode performance. Thus, the composition of the composite anode in the following

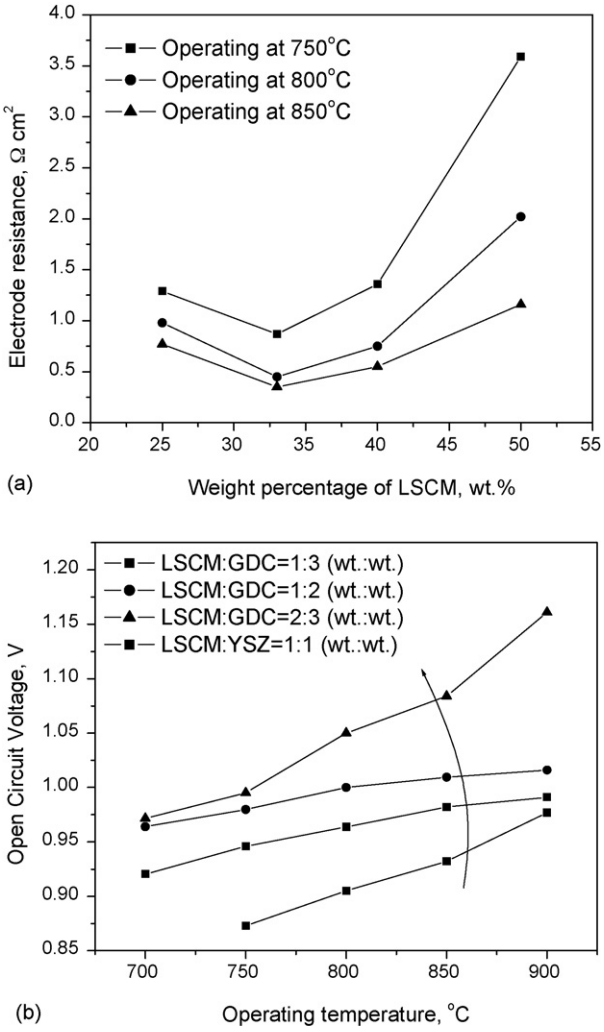

Fig. 3. Performance of LSCM/GDC composite anode in humidified CH_4. (a) Electrode resistance as function of LSCM weight percentage and (b) open-circuit-voltage of composite anode.

investigations, was fixed at 33 wt.% of LSCM and 67 wt.% of GDC, i.e., LSCM:GDC = 1:2 (w/w).

The open-circuit voltage (OCV) of the LSCM/GDC and LSCM/YSZ composite anodes in wet CH_4 at various temperatures as shown in Fig. 3(b). The GDC has moderate reforming activity while the YSZ is almost inert towards CH_4 steam-reforming. As a result, the LSCM/GDC composite is found to have much higher OCV than a LSCM/YSZ composite anode in wet CH_4. Furthermore, the results in Fig. 3(b) indicated that the more the LSCM in the composite anode, the higher is the OCV, which may be due to the higher catalytic activity of LSCM with that of GDC. A high content compared of LSCM could promote the internal reforming of humidified methane in the anode and thus increase the open-circuit voltage. In contract to the trend observed with hydrogen, the OCV of the composite anode in humidified CH_4 increases with the operating temperature, irrespective of the electrode composition. The observed OCV is much lower than the theoretical value calculated under equilibrium conditions [24] and indicates the slow reforming processes of humidified methane in the composite anode. A high tempera-

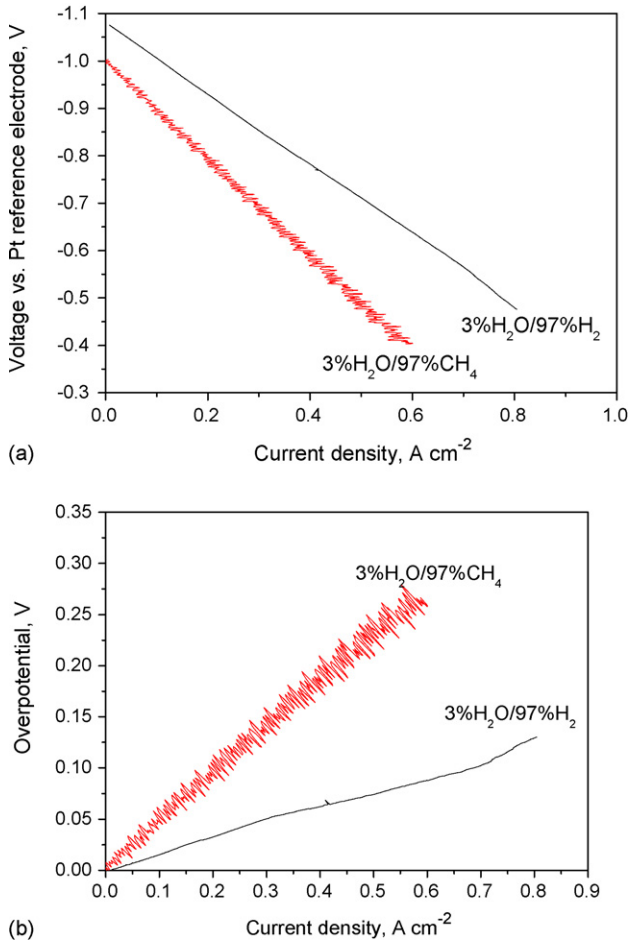

Fig. 4. (a) Polarization and (b) overpotential of LSCM/GDC composite anode with composition of LSCM:GDC = 1:2 (w/w) in wet H_2 and CH_4 at 850 °C.

ture is desirable for the composite anode to speed up the methane reforming, which results in a higher open-circuit voltage.

The anodic polarization of the LSCM/GDC composite anode in wet H_2 and CH_4 was measured with respect to the air solidus Pt reference electrode. As shown in Fig. 4(a), the OCV of the composite anode in wet H_2 and CH_4 at 850 °C is 1.076 and 1.003 V, respectively. The value in wet CH_4 is much lower than the corresponding theoretical value of 1.32 V (calculated at gas composition of 3% H_2O/97% CH_4) [24] and this shows that the LSCM/GDC composite anode has very poor steam-reforming activity towards CH_4. The polarization curve oscillates in wet CH_4. This phenomenon was also observed on GDC–impregnated LSCM anodes [25] and was attributed to the high surface-exchange properties for oxygen on doped CeO_2, and to possible synergistic processes involving the injection of mobile charged oxygen surface species to and from the GDC ionic carrier. The composite anode displays much higher performance in wet H_2 than in wet CH_4. At 0.5 V (with respective to the air Pt reference electrode without ohmic compensation), output current densities of 0.77 and 0.48 A cm^{-2} are observed in wet H_2 and CH_4, respectively. After compensating for the electrolyte ohmic loss and removing the OCV of the polarization curves in Fig. 4(a), one can obtain the overpotential vs. current density relationship (shown in Fig. 4(b)) of the LSCM/GDC composite anode in wet H_2 and CH_4. The results demonstrate the promising performance of the LSCM/GDC composite anode. At an output current density of 0.5 A cm^{-2}, the overpotential in wet H_2 and CH_4 at 850 °C is 0.073 and 0.248 V (i.e., an electrode resistance of 0.146 and 0.496 Ω cm^2), respectively.

3.2. Impedance response of LSCM–GDC composite anode in wet H_2 and CH_4

Experiments were performed under different operating temperatures and a dc bias in order to elucidate the oxidation reactions of wet H_2 and CH_4 on the LSCM/GDC composite anode. The resulting impedance spectra as a function of operating temperature are presented in Fig. 5. Though the absolute values are different, two depressed semi-circles can be observed in the impedance spectra obtained in wet H_2 and CH_4. These can be fitted to an equivalent circuit of $R_e(R_HQ_H)(R_LQ_L)$, where R_e is the resistance between the anode and the reference electrode, and (R_HQ_H) and (R_LQ_L) correspond to the high and low frequency arc, respectively. Hydrogen oxidation on a nickel electrode is well understood and is generally considered to involve

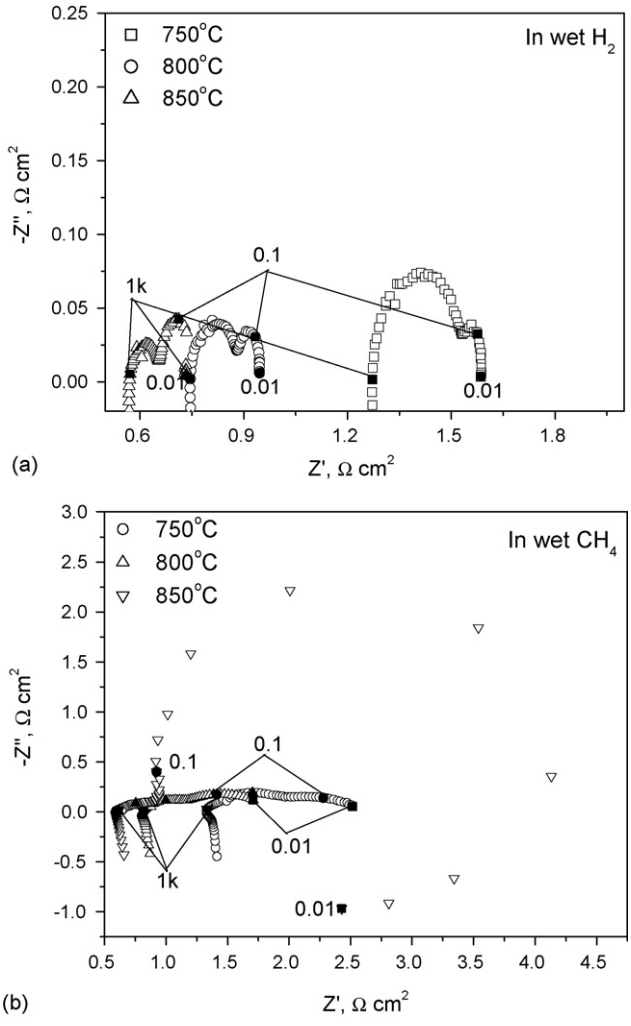

Fig. 5. Impedance responses of LSCM/GDC composite anode in (a) wet H_2 and (b) wet CH_4 under different operating temperatures.

gas diffusion, dissociation/adsorption of H_2, surface diffusion of the adsorbed species to the triple-phase-boundary (TPB), charge-transfer at the TPB and formation of water with the oxygen ions transported through the electrolyte. Several steps could be rate-determining depending on material properties and microstructure, atmosphere, temperature and current density. Jiang and Badwal [26] proposed the following reaction mechanism for hydrogen oxidation on a nickel electrode: (i) hydrogen dissociation is very fast at the SOFC operating temperature; (ii) surface diffusion and charge-transfer are the rate-determining steps; (iii) produce water can speed up the surface diffusion via a spillover mechanism. Unfortunately, this mechanism cannot explain the negative activation energy observed for the low-frequency arc. It has been reported [27] that the surface adsorption of chemical species on the metal surface is very weak and decreases with increasing temperature, as can be explained by gas kinetic theory. A similar explanation can be applied to the LSCM/GDC composite anode, namely: the higher the temperature, the lower is the surface adsorption on the LSCM (or GDC) particle surface. As a result, the actual concentration of adsorbed species at elevated temperature is likely to be the rate-determining step for H_2 and CH_4 oxidation.

When the LSCM/GDC composite anode is exposed to a wet CH_4 atmosphere, typical pseudo-inductive behaviour is observed in the low-frequency arc at an operating temperature of 850 °C (Fig. 5(b)). The impedance in the frequency range of 1–0.01 Hz appears as a large arc in the first quadrant and a small arc in the fourth quadrant. The large low-frequency arc and the pseudo-inductive behaviour of the impedance in wet CH_4 is similar to that observed for a direct methanol fuel cell (DMFC) [28,29], which suggests that some intermediate species may be produced at temperatures above 850 °C and subsequently poison the LSCM anode when CH_4 is used as the fuel. At present, we are unable to provide a convincing explanation for such behaviour. Mass spectroscopy and gas chromatography will be employed in future studies to measure the composition of the anode exhaust gas and these by elucidate the origin of the phenomena observed in Fig. 5(b).

Impedance spectra of the LSCM–GDC composite anode in wet CH_4 under dc bias are shown in Fig. 6. Both low-frequency arcs (one in the first quadrant and the other in the fourth quadrant in the frequency range of 1–0.01 Hz) decrease abruptly with increase in dc bias, whereas the high-frequency arc (from 10 kHz to 1 Hz) remains almost unchanged. The pseudo-inductive behaviour appearing at all the measured potentials suggests that at least two or three adsorbed intermediates are involved in the competing electro-oxidation processes that are taking place on the anode. If the large low-frequency arc is attributed to poisoning by some intermediates that are formed at a temperature above 850 °C in wet CH_4, the changes in impedance under dc, bias indicate that the poisoning species could be easily electro-oxidized under anodic polarization. No significant changes in impedance are found when the applied dc bias is higher than 200 mV, and this indicates that poisoning intermediate species may dominate the anode performance at low anodic polarization, while other adsorbed intermediate species, such as H_{ads} and $CH_{x,ads}$, may be present of high anodic

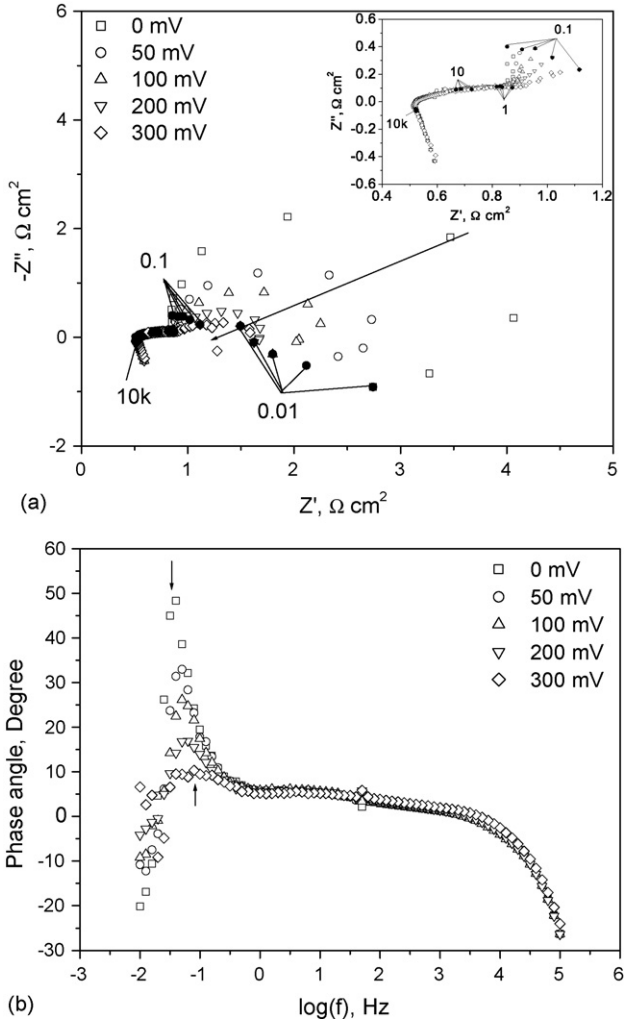

Fig. 6. Impedance spectra of the LSCM–GDC anode in wet CH_4 as function of dc bias at 850 °C: (a) Nyquist plot; (b) Bode plot.

polarization. Bode plots of the impedance in wet CH_4 under dc bias are shown in Fig. 6(b). The higher the dc bias, the lower is the phase angle in the frequency range of 1–0.01 Hz; this behaviour is reversed in the frequency range of 10 to 10^4 Hz. The characteristic frequency in the range 1–0.01 Hz shifts from 0.039 to 0.158 Hz with increasing dc bias from 0 to 300 mV. The other characteristic frequency (corresponding to the high-frequency arc), 16.6 Hz, is independent of the applied dc bias.

3.3. Stability of LSCM–GDC composite anode under current loading cycles

As shown in Fig. 7, the stability of the LSCM/GDC composite anode in wet CH_4 at 850 °C has been evaluated under different current loadings for an operating period of 50 h. A current density of 200 and 400 mA cm^{-2} was alternatively applied to the anode at time intervals of 10 h. The anode voltage was taken with respect to the Pt reference electrode. Except for some noise during the testing, the LSCM–GDC composite anode remains quite stable under polarization in wet CH_4. At a current density of 200 mA cm^2 the anode voltage is −0.85 V at the end of

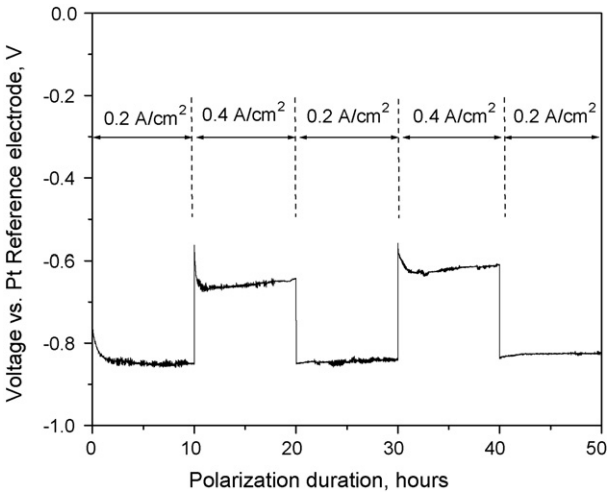

Fig. 7. Stability of LSCM/GDC composite anode under loading cycles in wet CH_4 at 850 °C.

the first 10 h of operation, and −0.825 V after 50 h of operation. It also should be noted from the polarization curves that the anode is initially activated under polarization, which may be partially attributed to water generation under anodic polarization that leads to high coverage of the surface with fuel at the reaction sites. On the other hand, it has been reported [22] that the conductivity of the LSCM material increases with increase of oxygen partial pressure. The water generated under anodic polarization will increase the oxygen partial pressure, and subsequently enhance the conductivity of the LSCM anode. Thus, the initial performance improvement of the composite anode under anodic polarization can be associated with the combined effect of the above two factors.

The morphology of the LSCM/GDC composite anode before and after 50 h of testing in wet CH_4 at 850 °C is shown in Fig. 8. The anode has a good microstructure of uniform particle size of less than 1 μm that has high porosity and good contact with the electrolyte. As shown in Fig. 8(a and b), no obvious microstructure changes and no carbon deposition on the LSCM/GDC composite anode after 50 h exposure in wet CH_4 are found. This shows that the developed LSCM/GDC composite anode possesses electrochemical performance comparable with the Ni cermet and can effectively suppress the carbon deposition when weakly humidified CH_4 is used as fuel.

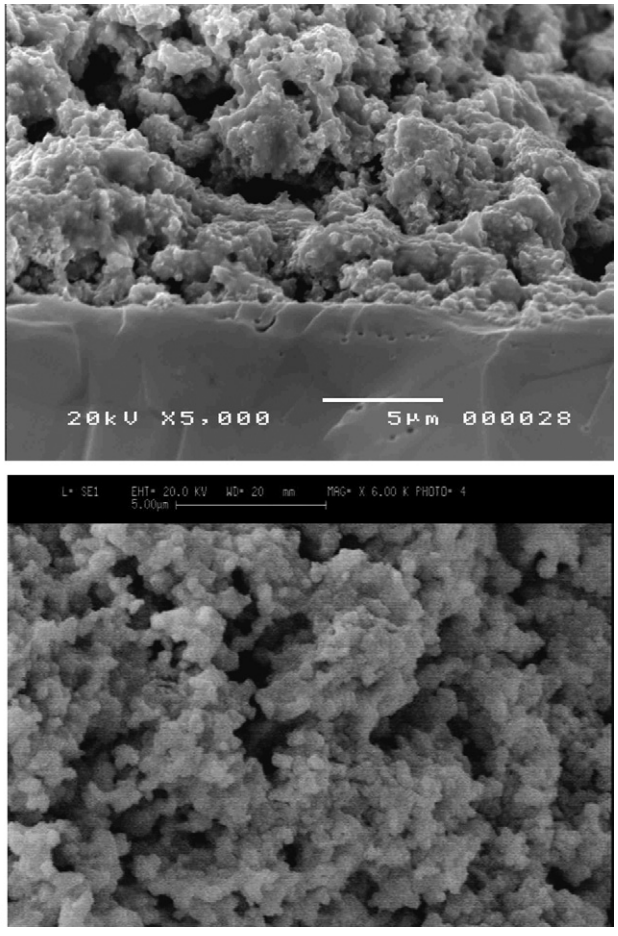

Fig. 8. Morphology of LSCM/GDC composite anode (a) before and (b) after 50 h of stability testing.

4. Conclusions

$La_{0.75}Sr_{0.25}Cr_{0.5}Mn_{0.5}O_3$ perovskite powder with fine particle size is synthesized through a combined citrate and EDTA complexing method. The optimum composition of the LSCM–GDC composite anode is 33 wt.% LSCM and 67 wt.% GDC. At an output current density of 0.5 A cm^{-2}, the overpotential of the composite anode in wet H_2 and wet CH_4 at 850 °C is 0.073 and 0.248 V (i.e., an anodic resistance of 0.146 and 0.496 Ω cm^2), respectively. This shows that the LSCM/GDC composite anode is a promising anode for the oxidation of H_2 and CH_4. Electrochemical impedance spectroscopy is measured as a function of operating temperature and dc bias to understand the oxidation pathway of CH_4 on the LSCM/GDC composite anode. The results indicate that the developed LSCM/GDC composite anode can effectively suppress carbon deposition when using weakly humidified CH_4 and possesses an electrochemical performance that is comparable with a Ni cermet.

Acknowledgements

The authors would like to appreciate the financial support from the Singapore Millennium Foundation and US Army Communications-Electronics Research Development and Engineering Center.

References

[1] P.S. Maiya, T.J. Anderson, R.L. Mieville, J.T. Dusek, J.J. Picciolo, U. Balachandran, Appl. Catal. A: Gen. 65 (2000) 196.
[2] M. Radecka, Thin Solid Films 98 (2004) 451.
[3] P.R. Mishra, P.K. Shukla, A.K. Singh, O.N. Srivastava, Int. J. Hydrogen Energy 28 (2003) 1089.
[4] S.W. Zha, A. Moore, H. Abernathy, M.L. Liu, J. Electrochem. Soc. 151 (2004) A1128.
[5] S. Primdahl, J.R. Hansen, L. Grahl-Madsen, P.H. Larsen, J. Electrochem. Soc. 148 (2001) A74.

[6] S.P. Yoon, J. Han, S.W. Nam, T.H. Lim, S.A. Hong, J. Power Sources 136 (2004) 30.
[7] J. Akikusa, K. Adachi, K. Hoshino, T. Ishihara, Y. Takita, J. Electrochem. Soc. 148 (2001) A1275.
[8] Y. Tabata, H. Orui, K. Watanabe, R. Chiba, M. Arakawa, Y. Yamazaki, J. Electrochem. Soc. 151 (2004) A418.
[9] A. Sin, E. Kopnin, Y. Dubitsky, A. Zaopo, A.S. Aricò, L.R. Gullo, D. La Rosa, V. Antonucci, J. Power Sources 145 (2005) 68.
[10] Z.L. Zhan, Y.B. Lin, M. Pillai, I. Kim, Scott A. Barnett, J. Power Sources 161 (2006) 460.
[11] H. Kim, C. Lu, W.L. Worrell, J.M. Vohs, R.J. Gorte, J. Electrochem. Soc. 149 (2002) A247.
[12] C. Lu, W.L. Worrell, C. Wang, S. Park, H. Kim, J.M. Vohs, R.J. Gorte, Solid State Ionics 152 (2002) 393.
[13] C. Lu, W.L. Worrell, R.J. Gorte, J.M. Vohs, J. Electrochem. Soc. 150 (2003) A354.
[14] S. Park, J.M. Vohs, R.J. Gorte, Nature 404 (2000) 265.
[15] A.L. Sauvet, J. Fouletier, F. Gaillard, M. Primet, J. Catal. 209 (2002) 25.
[16] A.L. Sauvet, J.T.S. Irvine, Solid State Ionics 167 (2004) 1.
[17] S.W. Tao, J.T.S. Irvine, Chem. Mater. 16 (2004) 4116.
[18] G. Pudmich, B.A. Boukamp, M. Gonzalez-Cuenca, W. Jungen, W. Zipprich, F. Tietz, Solid State Ionics 135 (2000) 433.
[19] S. Primdahl, J.R. Hansen, L. Grahl-Madsen, P.H. Larsen, J. Electrochem. Soc. 148 (2001) A74.
[20] S.W. Tao, J.T.S. Irvine, Nat. Mater. 2 (2003) 320.
[21] J. Liu, B.D. Madsen, Z.Q. Ji, S.A. Barnett, Electrochem. Solid-State Lett. 5 (2002) A122.
[22] S.W. Tao, J.T.S. Irvine, J. Electrochem. Soc. 151 (2004) A252.
[23] X.J. Chen, S.H. Chan, K.A. Khor, Electrochim. Acta 49 (2004) 1851.
[24] S.P. Jiang, X.J. Chen, S.H. Chan, J.T. Kwok, K.A. Khor, Solid State Ionics 177 (2006) 149.
[25] S.P. Jiang, X.J. Chen, S.H. Chan, J.T. Kwok, J. Electrochem. Soc. 153 (2006) A850.
[26] S.P. Jiang, S.P.S. Badwal, J. Electrochem. Soc. 144 (1997) 3777.
[27] K. Christmann, Surf. Sci. Rep. 9 (1988) 1.
[28] I.M. Hsing, X. Wang, Y.J. Leng, J. Electrochem. Soc. 149 (2002) A615.
[29] R.C. Jiang, H.R. Kunz, J.M. Fenton, J. Electrochem. Soc. 152 (2005) A1329.